Available on CMS information server

CMS NOTE 2000/062

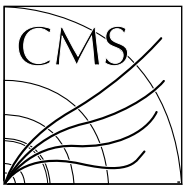

The Compact Muon Solenoid Experiment

CMS Note

Mailing address: CMS CERN, CH-1211 GENEVA 23, Switzerland

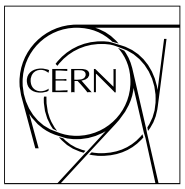

24 July 2000

Investigation of the charge collection for strongly irradiated Silicon strip detectors of the CMS ECAL Preshower

Ph. Bloch, A. Peisert
CERN, Geneva, Switzerland

Y.H. Chang, A.E. Chen, S. Hou, W.T. Lin
National Central University, Chungli, Taiwan

A.E. Cheremukhin, I.A. Golutvin, A.R. Urkinbaev [a)], N.I. Zamiatin
Joint Institute for Nuclear Research, Dubna, Russian Federation

Abstract

Strongly irradiated silicon strip detectors of different size, thickness and different design options were tested in a muon beam at CERN in 1999. A charge collection efficiency in excess of 85% and a signal to noise ratio of 6 are obtained in all cases at high enough bias voltage. Details of the charge collection in the inter-strip and the guard ring region and crosstalk between strips were also studied. We find that the charge collection efficiency and the cross talk between strips depend on the inter-strip distance.

[a)] On leave of absence from INP, Tashkent

1 Introduction

The expected high hadron fluence in the silicon strip detectors of the CMS Preshower detector requires careful design of the sensors. During and after irradiation, the sensors will suffer surface damage, bulk damage and changes of the doping concentration. The aim of the test in July 1999 using a precision telescope was to study the charge collection efficiency (CCE) for irradiated detectors of various topologies.

Many measurements on the charge collection of irradiated Preshower detectors have already been done in the laboratory using a ^{106}Ru radioactive source [1]. However the geometry and trigger conditions with the source are less precise than in a beam and do not allow us to study fine details such as the collection in the inter-strip or the guard ring region. We have already shown with non-irradiated detectors that detailed studies can be performed in a high energy beam using a precise telescope [2].

Nine detectors were studied during the run in 1999; we present here the main results of this test.

2 Experimental set-up description

A schematic view of the experimental set-up is shown in Fig. 1. A beam telescope, provided by the Taiwanese group, consisting of 10 micro-strip detectors read by a Viking chip [3], was inserted inside a commercial freezer. This telescope allowed to reconstruct tracks in 2 dimensions with a precision of the order of 10 micrometers. Silicon Preshower detectors (at maximum 2 at a time) were inserted in the middle of the telescope.

These silicon detectors were read at $40MHz$ sampling rate with the SCT32 [4] chip, connected through a discrete array of capacitances in order to cope with the large bulk current due to irradiation. The temperature regulation of the fridge was set to the minimum ($-30°C$) to reduce the leakage current and therefore maximise the signal-to-noise ratio. There was no active cooling (only the fridge convection), so the exact temperature of the detectors in presence of electronics was$\approx -20°C$, but the leakage current was always very stable.

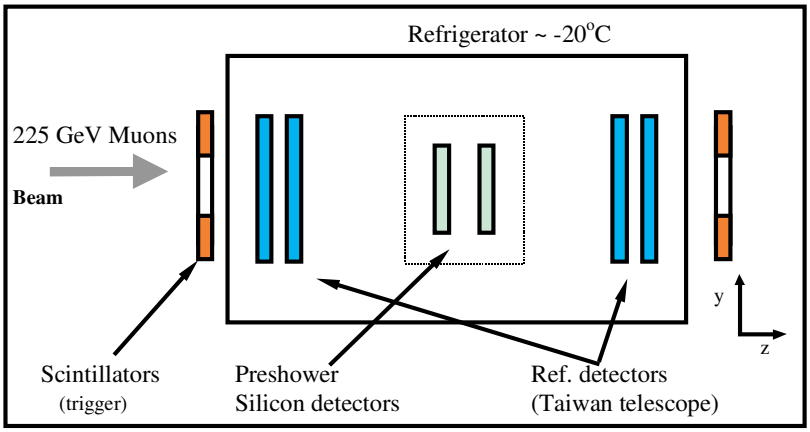

Figure 1: Schematic of the experimental set-up.

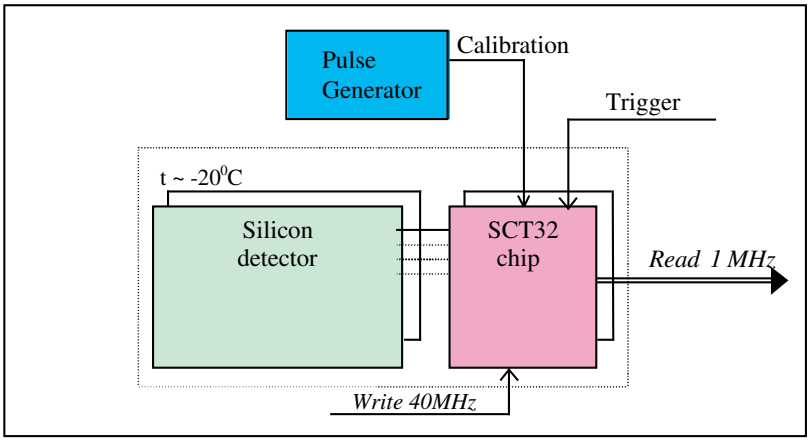

Figure 2: Scheme of the read-out systems.

An $8ns$ wide coincidence was required between the $40MHz$ clock and the particle trigger provided by scintillators, in order to select particles with a well defined phase relative to the clock. A sketch of the readout system is shown in Fig. 2. A pulse generator was used for calibration runs during periods without beam. The channel calibration of the SCT32 chip was done without disconnecting it from the Si-detector.

With the four scintillation counters it was possible to vary the beam spot at the face of the studied Silicon sensors. We used:

- a 4 fold coincidence to select a small squared area ($\approx 10 \times 10 mm^2$),
- a 2 fold vertical coincidence to select a $30 \times 10 mm^2$ area running along the strip length,
- a 2 fold horizontal coincidence to select a $10 \times 30 mm^2$ area running across a large number of strips.

In each case, the detectors were put in two different geometrical positions: either well centred on the beam or placed in such a way that the beam hit the last 6 strips and the corner of the detector. This last set of data can be used to study the charge collection close to the guard rings. Figure 3 shows the beam spot relative to the sensor active area for four such corner runs. One sees that the beam spot did not always cover fully the detector corner so that the efficiency near the guard ring could in some cases only be studied in one direction (either x along the strips or y across the strips).

Data were taken parasitically to a CMS $225 GeV/c$ muon test run at the H2 area of the CERN SPS. About 2 Million events were recorded, corresponding to 250 different conditions (various detectors, bias, positions).

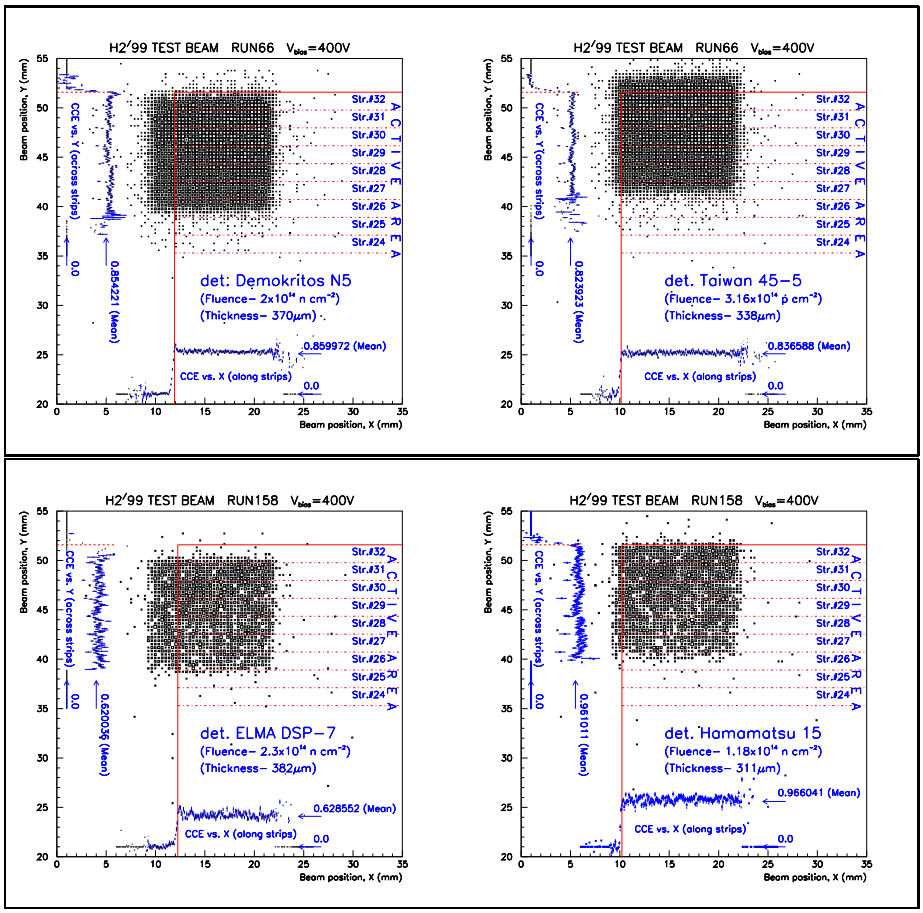

Figure 3: Beam spot distributions and CCE distributions in two directions.

3 Si-strip detector samples

Six sets of detectors were inserted in turn in the telescope. Unfortunately, the second read-out electronics card died slowly during the run so that the data of 3 detectors can not be used. All except detector Hamamatsu 103 ($\rho = 0.9 k\Omega \times cm$) have a resistivity higher than $4 k\Omega \times cm$. All the detectors had been pre-irradiated before, either at CERN-PS with 24 GeV protons or in Dubna [5] with fast neutrons, and kept at low temperature after irradiation (details on our irradiation facilities and procedures can be found in [1]).

The cross-section of one of the detectors (Elma N9-1) is shown in Fig. 4. From left to right on sees the scribe line, four aluminized guard rings (GR) and the aluminized strips with a p^+ implant. Important parameters are the sensor thickness, the inter-strip and the inter-implant distances . Table 1 summarizes the characteristics of each

Table 1: Main characteristics of tested detectors.

Detector	Fluence $(\times 10^{14} cm^{-2})$	V_{fd} (V)	Distance p+ to p+ (μm)	Distance Al to Al (μm)	Thickness (μm)	Dimension (mm)	Pitch size (mm)
Hamamatsu 8	non-irradiated	60	110	70	313	60×60	1.81
Hamamatsu 15	1.18 n	149	110	70	311	60×60	1.81
Hamamatsu 103	0.96 n	32	110	70	322	60×60	1.81
DSP 7 (Elma)	2.30 n	509	120	80	382	60×60	1.81
D2-1-n+ (Elma)	1.18 n	133	120	80	308	60×60	1.81
Taiwan 45-5	3.16 p	241	50 160	40 150	338	60×60	1.81
Takion-3	2.10 n	320	the same as previous		320	60×60	1.81
N9-1 (Elma)	3.16 p	214	60	40	300	63×63	1.90
N5 (Greece)	2.00 n	431	160	160	370	60×60	1.81

detector, as well as the fluence they received before the test and the full depletion voltage obtained from a CV curve at $5kHz$. The neutron fluences are expressed in '1MeV neutron equivalent' unit. For the 24GeV protons, we quote the received proton fluence: the '1MeV neutron equivalent' fluence can be obtained by dividing it by a factor of approximately 2. The Taiwan and Takion detectors are multi-geometry sensors with different inter-strip distances.

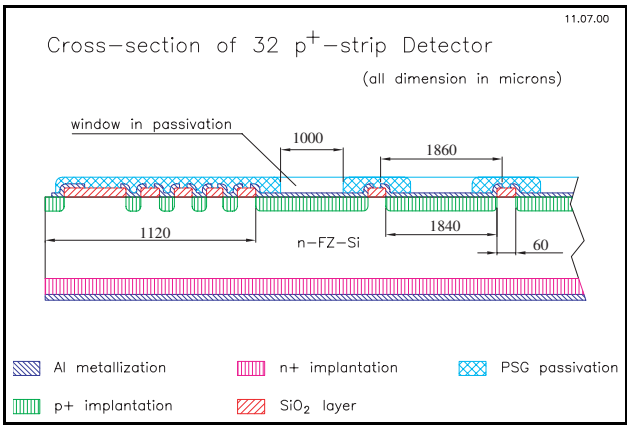

Figure 4: A cross-section of the Si-strip detector.

4 Test pulse calibration

For each detector, data were recorded with a calibrated pulse injection at a high enough bias voltage to be fully depleted. The timing of the test pulse was varied by steps of $12.5ns$, and the calibration is obtained from the highest signal observed. An attempt was also made to fit the shape of the pulse with a function of the form

$$f(t) = (b(t - t_0))^{a-1} e^{-b(t-t_0)}$$

and to take the function maximum: the results are similar within a few percents but somewhat less reliable. The injected charge was nominally $6.8fC$ ($68mV$ on $0.1pF$). Since a minimum ionising particle should deposit $4fC$ in a $300\mu m$ thick detector, we arbitrarily divide the calibration charge by a factor 1.7 to express our results in mip (minimum ionising particle). The value of the injection capacitor (directly on chip) is known to be uniform between channels, but its absolute value may vary from one ASIC production to the next. Our normalisation may therefore be easily wrong by 20%. To overcome this difficulty, we have also measured a non irradiated detector, and we determine an overall factor (later applied to all the data) in order to get exactly $1mip$ for the non-irradiated detector at high bias ($500V$).

Figure 5 shows a typical output pulse produced by a step-like injection charge. The pulse varies by less than $\sim 3\%$ when one moves by $\pm 6ns$ around the maximum, showing that we are not sensitive to the remaining timing jitter between the clock and the trigger. Figure 6 and 7 show the effect of the calibration for data taken with one of the card (SCT2) which was particularly non-uniform [1)]: after calibration, the response is uniform with a dispersion

[1)] this non uniformity is a known defect of SCT32 and has been corrected in later versions such as the SCT 128

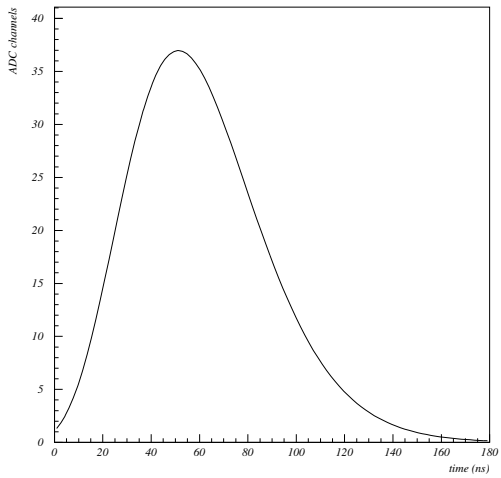

Figure 5: Output pulse produced by a step-like injection charge.

of less than 5%.

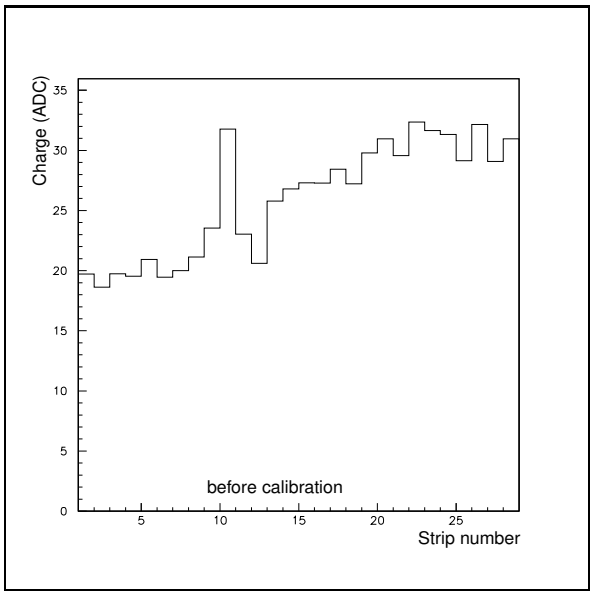

Figure 6: Muon signal as a function of the strip number before calibration.

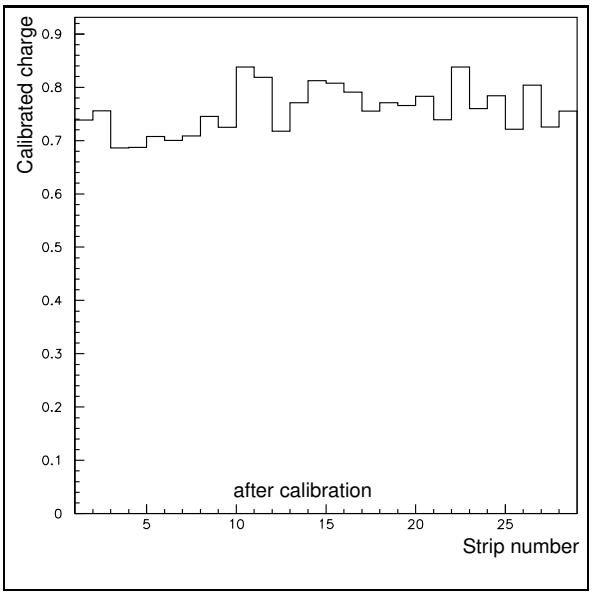

Figure 7: Muon signal as a function of the strip number after calibration.

5 Alignment of the detectors relative to telescope

The alignment of the detectors relative to the telescope is determined using a simple technique: in each event, for each Preshower detector, we select the strip with the highest charge and we plot the difference between the y coordinate (as measured from the telescope) and the position of the centre of the strip (as defined in the local coordinate of the Preshower silicon detector). The resulting distribution is shown on Fig. 8. We observe a nice rectangle with almost no background on the 2 sides, which has the width of one strip. The sharp edges of the distribution can be fitted with a step function, and the strip centre is defined as the mean of the position of the 2 edges. The pitch of the strips is very precisely known.

A single translation constant can be used for each detector. The position along the beam is optimised in order to have the same alignment constant for tracks with various slopes dy/dz (z being along the beam). Finally, a possible rotation in the $x - y$ plane is evaluated by redoing the alignment for different values of the telescope x coordinate. By fitting the slope of the edges of the distribution after alignment, one can estimate the overall geometrical precision. This is a pessimistic estimate, because the sharpness of the edges may be smeared by

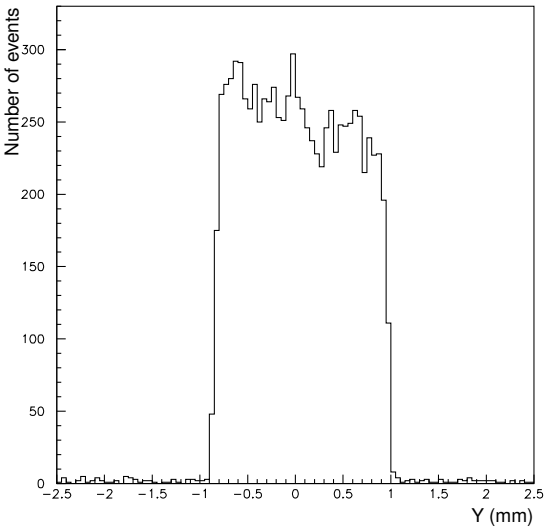

Figure 8: Telescope y coordinate for events hitting a given preshower strip.

other physical effects than the position resolution, for example by the charge sharing between strip implants. Nevertheless, in all the cases, we find a precision better than $16\mu m$.

6 Data analysis

Before detailed analysis, the data are processed through the following steps:

1. Pedestal computation. In an event, very few strips have a charge signal. The plot of the raw charge distribution exhibits therefore a large peak at zero charge which is fitted by a Gaussian curve to determine both the pedestal position and the noise for each individual run.

2. Common noise subtraction. The data suffer from low frequency external noise. This "common" noise (CN) can be easily removed event by event by identifying strips without signal (a signal is defined as a charge 2.5 sigmas above pedestal) and computing the average deviation from the pedestals. This procedure is most efficiently applied by dividing the detector in a few regions (3 to 5),

$$CN = \sum (EVT_i - PED_i)/n$$

   where EVT_i is the raw value of channel i, PED_i its pedestal and the sum extends to the n strips without signal of a given region. The signal of each strip is then redefined as:

$$SIGNAL_i = EVT_i - PED_i - CN$$

   The importance of this subtraction depends strongly on the external conditions.

3. Signal normalisation. The signal of each channel is then divided by the corresponding value of the calibration injection pulse (see section 4) to express it in mip.

4. Search for the central hit strip. There are two alternative ways to define the central hit strip: either by looking for the strip with the largest signal in the region hit by the beam (stand-alone method) or by defining the strip hit by the particle using the beam telescope information. We will explicitly mention in the following which algorithm has been used for each particular analysis.

5. Finally, the normalised charges of the central strip and of its neighbours (2 on each side) are written to an ntuple for a detailed analysis.

7 Charge collection efficiency versus Bias Voltage

7.1 Analysis in stand-alone mode

A first analysis was done in September 1999 before the telescope data were available. The Preshower silicon detector was scanned and the charge of the highest strip was retained as signal. The common noise subtraction was done using 5-strips wide regions. From the results on cross talk presented in section 8, it appears that this may have resulted in a slight underestimate of the charge, since the 2 neighbour strips have often been used for common noise subtraction. But the effect should be very small (maximum 2.5%) and was the same for the reference detector. The most probable value of the charge distribution was determined using a local Gaussian fit.

Figure 9 shows the most probable value of the charge distribution for the non-irradiated (reference) detector Hamamatsu 8 as a function of the bias voltage. An overall normalisation factor has been applied to obtain charge unity at V=500 V. The detector shows a full charge collection around 80V. Note that the reference data of Hamamatsu 8 had been taken without making a coincidence between trigger and clock, so that the arrival of the particle was random relative to the $40MHz$ clock. A cut has been applied on the ratio of the first to second time sample to ensure a good timing. The result of a run taken at a later stage with a proper timing is also shown on Fig. 9 and is in good agreement.

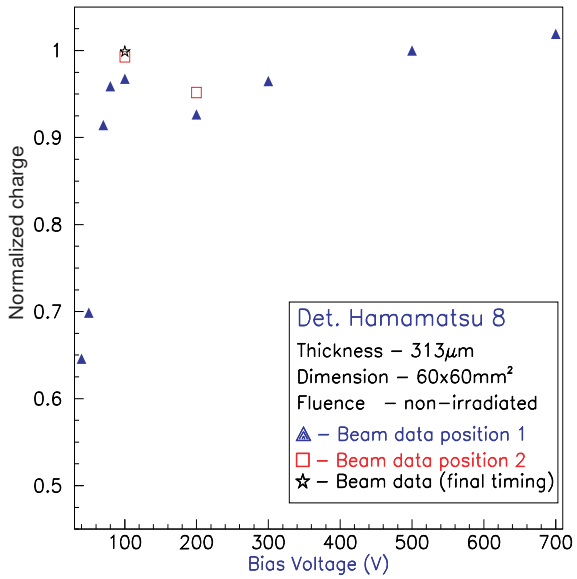

Figure 9: Normalised charge for the reference, non-irradiated detector Hamamatsu 8.

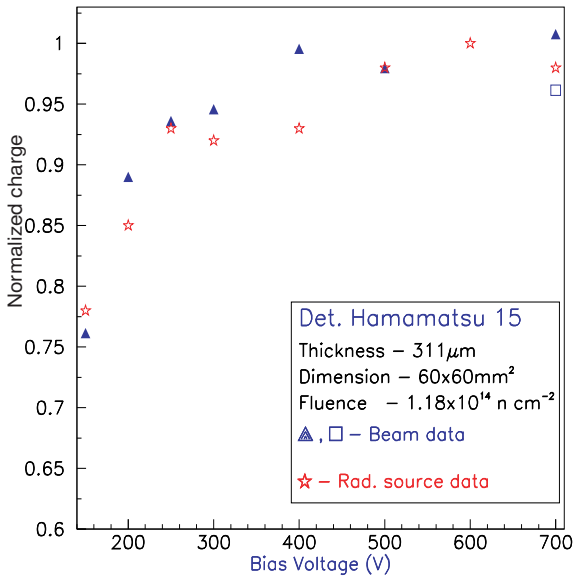

Figure 10: Normalised charge for the detector Hamamatsu 15.

The same procedure was subsequently applied to all other detectors. The measured charge has been corrected for calibration, the overall normalisation factor applied and finally the charge has been normalised to the thickness of Hamamatsu 8 ($313\mu m$). Figures 10 to 14 show the measurements obtained for the thin ($\sim 300\mu m$) detectors. The charge collection efficiency measured in the laboratory with the ^{106}Ru source is also shown. The shapes are in excellent agreement. The absolute values differ slightly , but we could not find any systematic deviation: the difference of efficiency on the plateau between the beam and the source measurement for the five plots of figures 10 to 14 has a dispersion of 5%, which we consider as a reasonable estimate of the uncertainty in the whole normalisation procedure.

Figures 15 and 16 show the charge collection efficiency for the 2 detectors which have a large thickness. It is clear that for heavily irradiated fat detectors, the efficiency plateau is difficult to reach. Surprisingly, there is in these 2 cases a bigger disagreement between the source and the beam normalisation (the results with the beam look too high) , but the shapes still agree very well.

7.2 Analysis using the telescope

All runs were later re-analysed using the telescope to define which strip should be used for the charge measurement. This method allows us to remove events with poor tracks or tracks outside the fiducial area. The rest of the procedure is identical as before. There is a good agreement between the two analysis. (compare Fig. 17 and

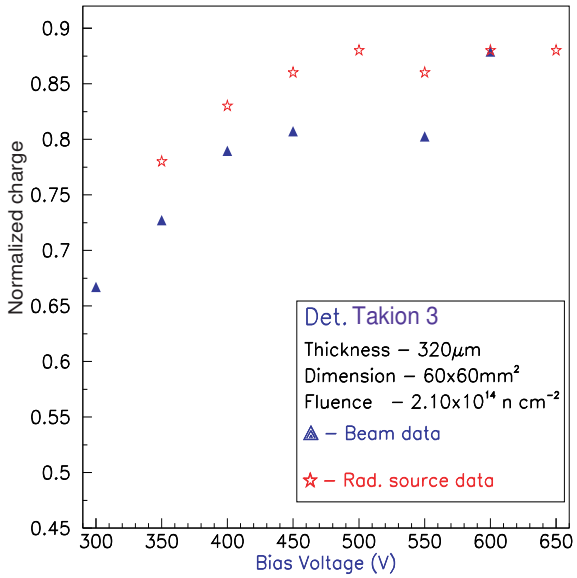

Figure 11: Normalised charge for the detector Takion 3.

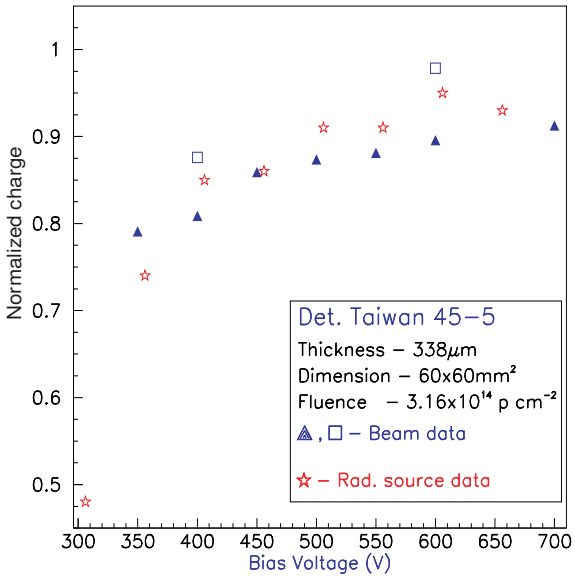

Figure 12: Normalised charge for the detector Taiwan 45-5.

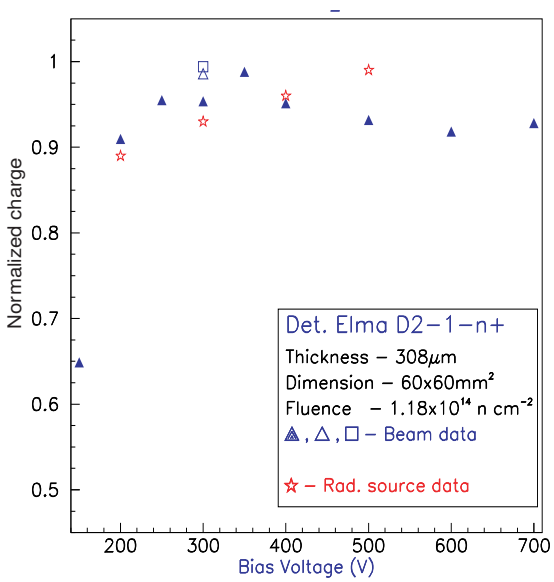

Figure 13: Normalised charge for the detector Elma d2-1-n^{+}.

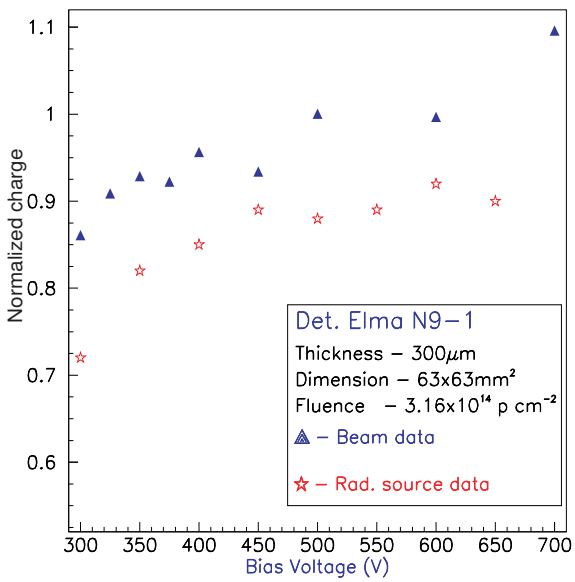

Figure 14: Normalised charge for the detector Elma N9-1.

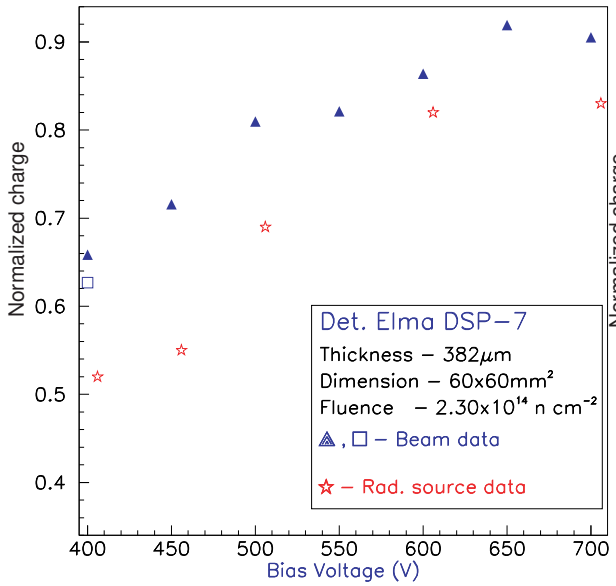

Figure 15: Normalised charge for the detector Elma DSP7

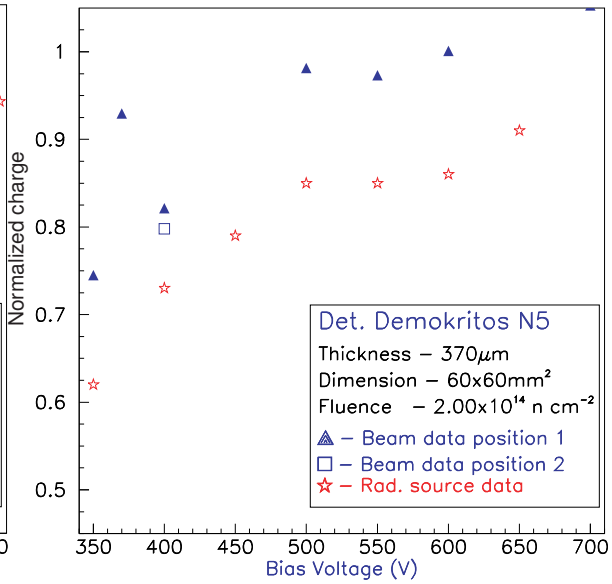

Figure 16: Normalised charge for the detector Demokritos N5.

Fig. 18 with Fig. 9 and Fig. 10 respectively).

7.3 Conclusions on charge collection vs. bias

The measurements done with the beam confirm the results obtained in the laboratory with a simpler setup using a radioactive source. A good plateau with an efficiency $> 85\%$ is always obtained for thin irradiated detectors.

8 Analysis of the charge in the central and neighbouring strips as function of particle position

8.1 Study of inter-strip region

In this analysis the central strip is defined as the strip which should be hit according to the telescope measurement. Figures 19 to 28 show the average value of the charge measured in the central strip and its two neighbours as a function of the track position for a few detectors, in steps of 20 microns. The average charge is computed in the interval from -1 and $+3$ normalised charges, to avoid fluctuations due to the long Landau tail. In each case we present two plots. The plot on the left shows the charge in the central strip (black dots), the charge of the strip on the left (open red circles) and on the right (green full triangles). The solid (resp. dashed) line shows the area covered by the p^+ implant (resp. the aluminization). The right plot shows the total charge of the "cluster" (summing the charge of 3 strips).

One observes that:

1. there is a clear charge loss on the strip edge regions if the bias is below the efficiency plateau. This is the case for Hamamatsu 8 at 40V (Fig. 36), d2-1-n+ at 150V (Fig. 38) and even more for N5 (Fig. 40), which is thick and never reaches a good plateau.

2. Once on efficiency plateau, the cluster charge is always very uniform inside the implant region (Figures 19 to 34).

3. In the inter-strip region one observes however even at high bias a small loss. This effect seems less pronounced if the distance between the Al lines is small (compare for example Figures 25 and 27 which show the small and large inter-strip regions of Taiwan45 at 400V).

To better quantify the last statement we have constructed the cluster charge distribution separating the data of each detector in only two sets (events inside or outside the implant region) and we plotted the ratio of either their most

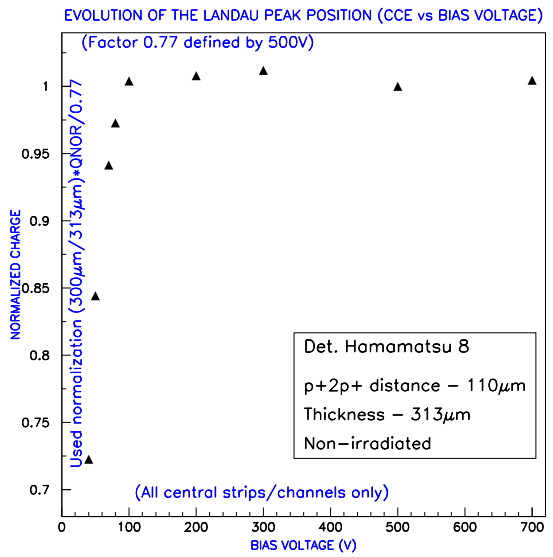

Figure 17: Normalised charge for the detector Hamamatsu 8 (with telescope)

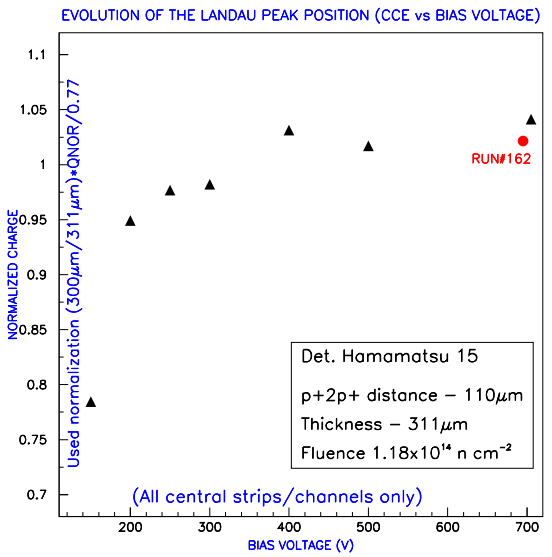

Figure 18: Normalised charge for the detector Hamammatsu 15 (with telescope).

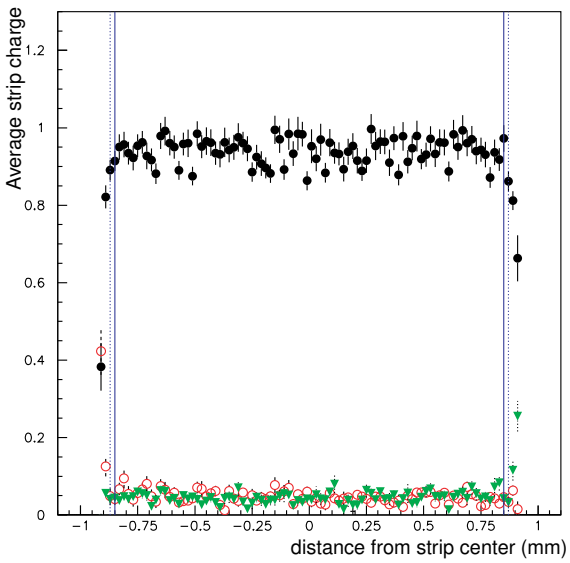

Figure 19: Average normalised strip charge as a function of the distance to the centre of the central strip for Hamamatsu 8 at 100 V.

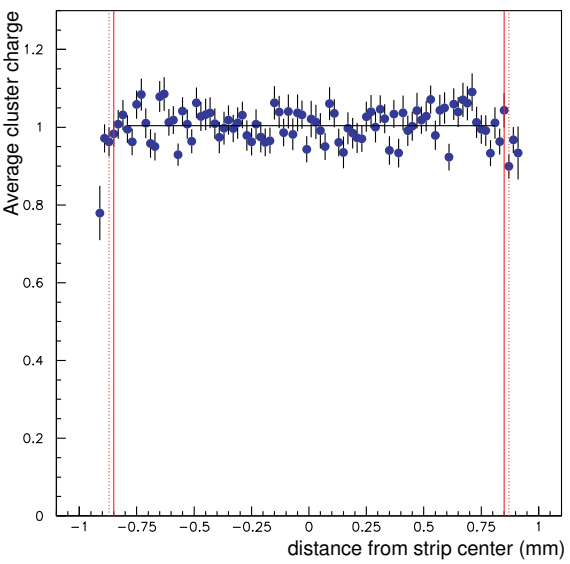

Figure 20: Average cluster normalised charge as a function of the distance to the centre of the central strip for Hamamatsu 8 at 100 V.

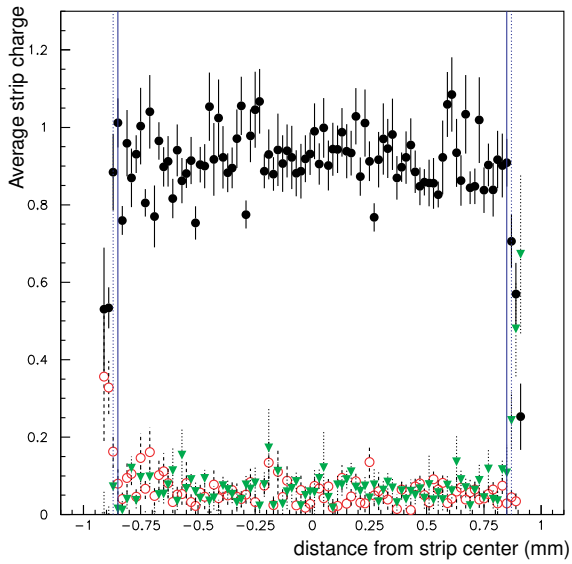

Figure 21: Average strip charge as a function of the distance to the center of the central strip for Hamamatsu 15 at 700 V.

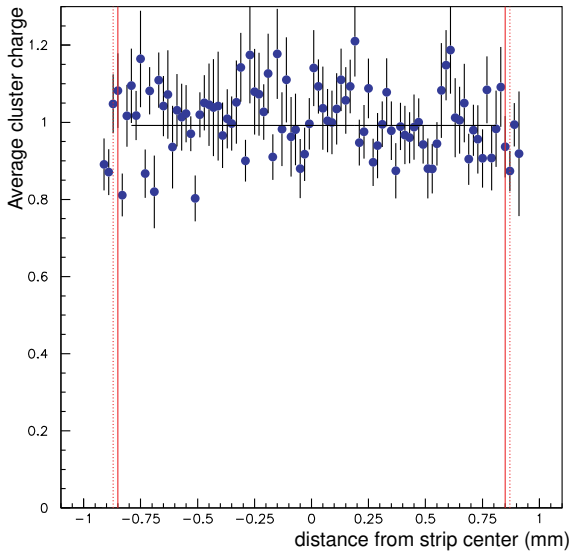

Figure 22: Average cluster charge as a function of the distance to the centre of the central strip for Hamamatsu 15 at 700 V.

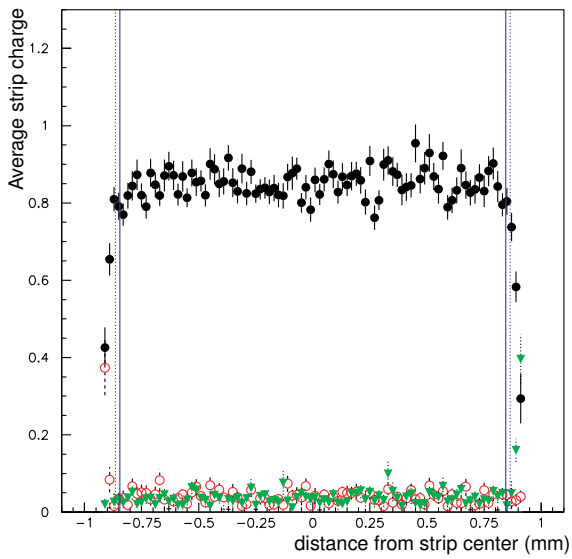

Figure 23: Average strip charge as a function of the distance to the centre of the central strip for D2-1-n$^+$ at 300V.

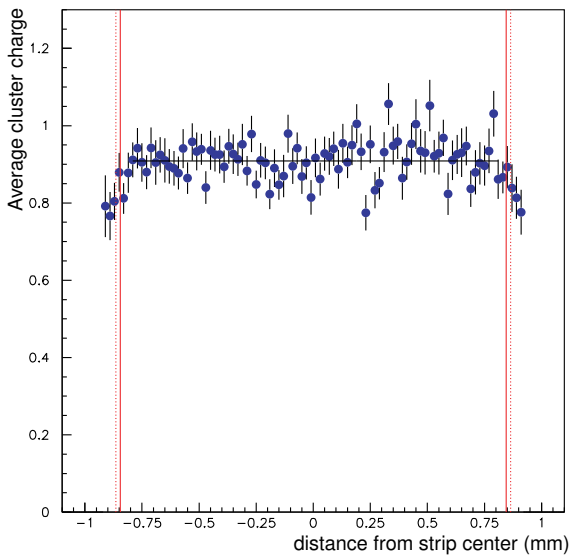

Figure 24: Average cluster charge as a function of the distance to the centre of the central strip for D2-1-n$^+$ at 300V.

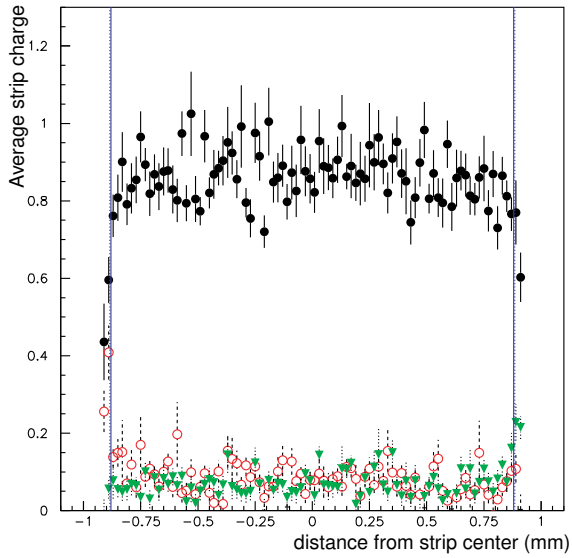

Figure 25: Average strip charge as a function of the distance to the centre of the central strip for Taiwan 45 at 400V., small inter-strip section

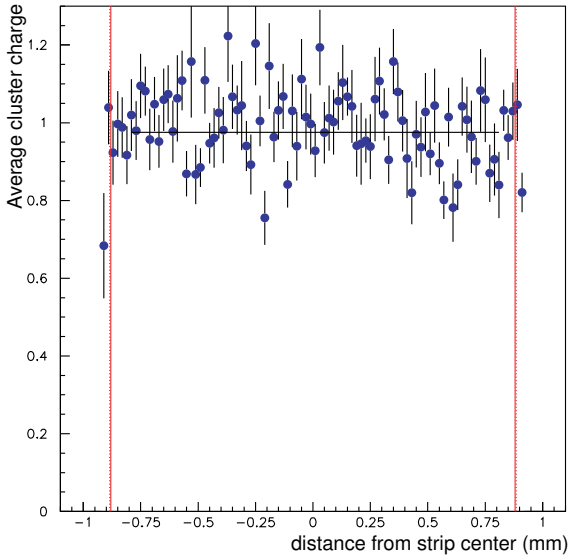

Figure 26: Average cluster charge as a function of the distance to the centre of the central strip for Taiwan 45 at 400V, small inter-strip section

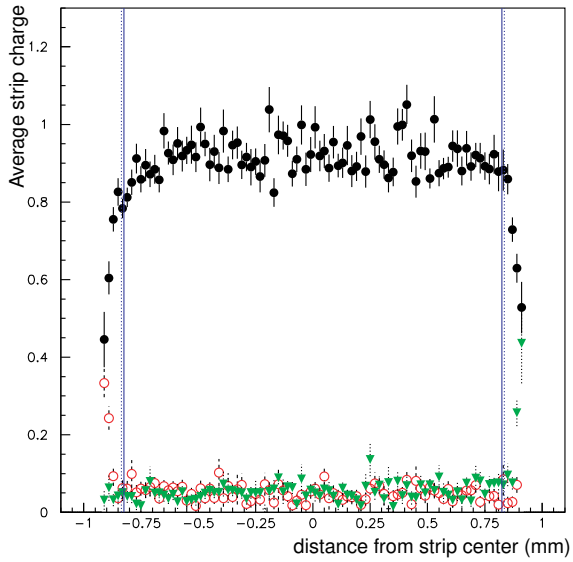

Figure 27: Average strip charge as a function of the distance to the centre of the central strip for Taiwan 45 at 400V., large inter-strip section

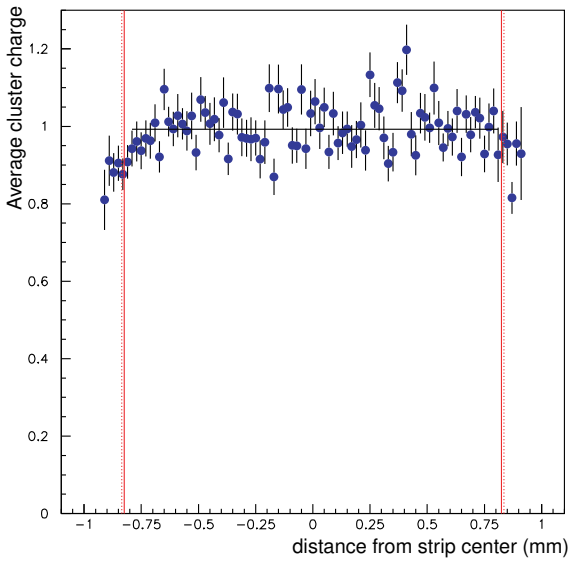

Figure 28: Average cluster charge as a function of the distance to the centre of the central strip for Taiwan 45 at 400V, large inter-strip section

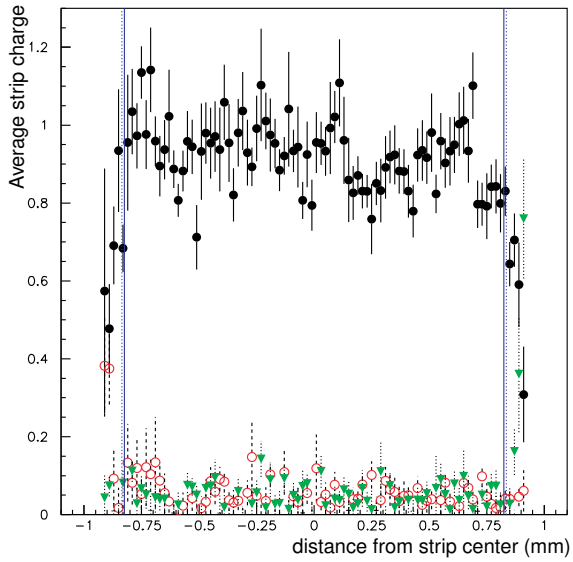

Figure 29: Average strip charge as a function of the distance to the centre of the central strip for Takion 3 at 500V., large inter-strip section

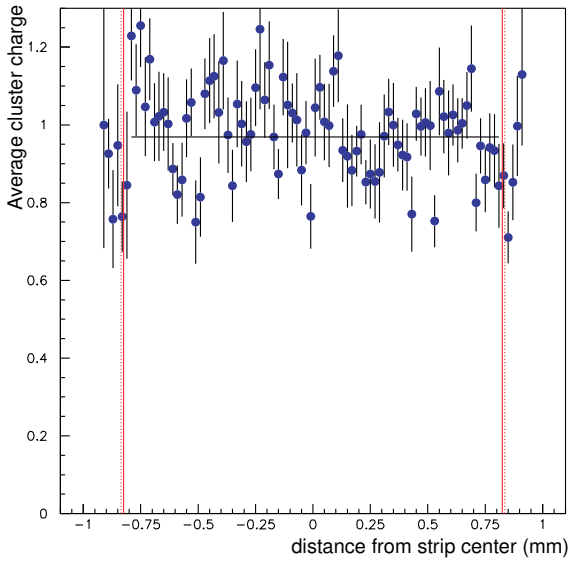

Figure 30: Average cluster charge as a function of the distance to the centre of the central strip for Takion 3 at 500V, large inter-strip section

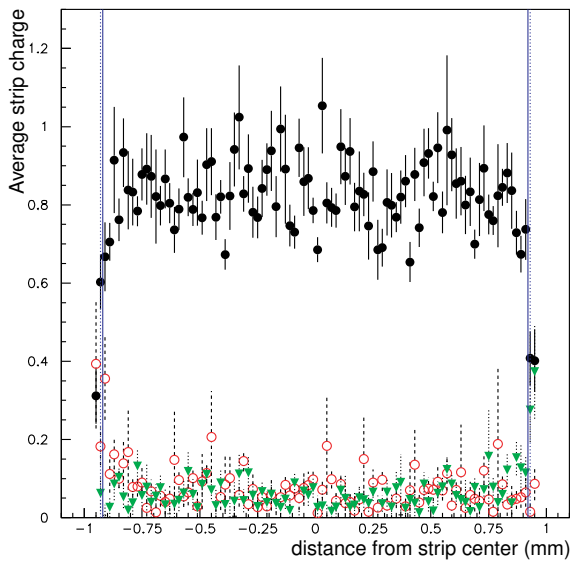

Figure 31: Average strip charge as a function of the distance to the centre of the central strip for Elma N9-1 at 450V.

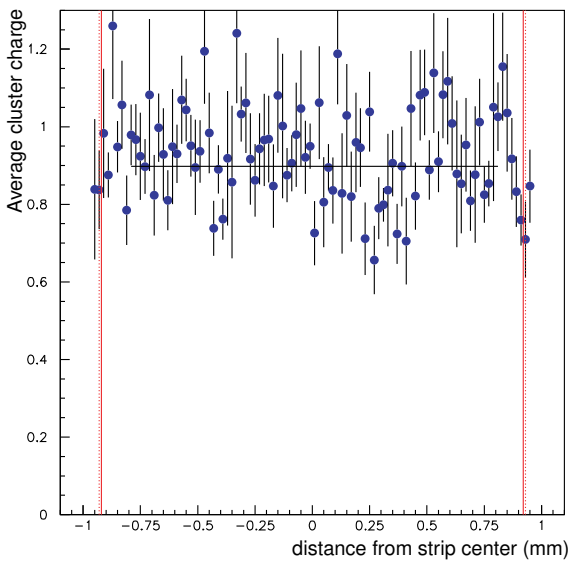

Figure 32: Average cluster charge as a function of the distance to the centre of the central strip for Elma N9-1 at 450V.

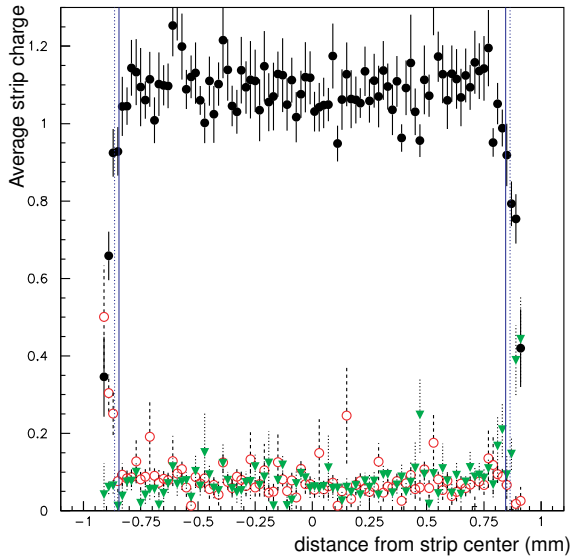

Figure 33: Average strip charge as a function of the distance to the centre of the central strip for Elma DSP7 at 650V.

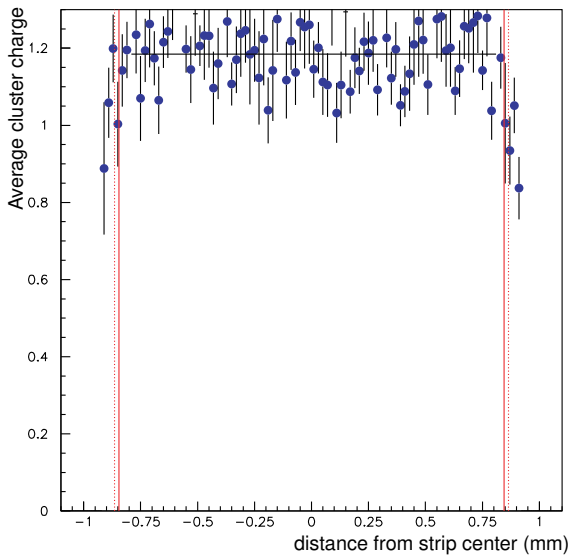

Figure 34: Average cluster charge as a function of the distance to the center of the central strip for Elma DSP7 at 650V.

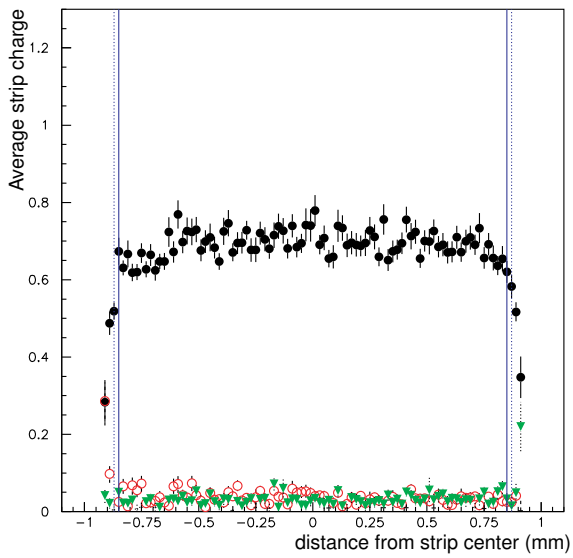

Figure 35: Average strip charge as a function of the distance to the centre of the central strip for Hamamatsu 8 at 40V.

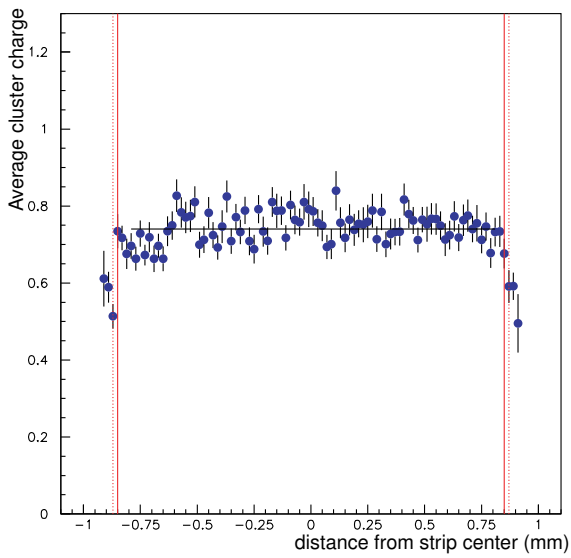

Figure 36: Average cluster charge as a function of the distance to the centre of the central strip for Hamamatsu 8 at 40V.

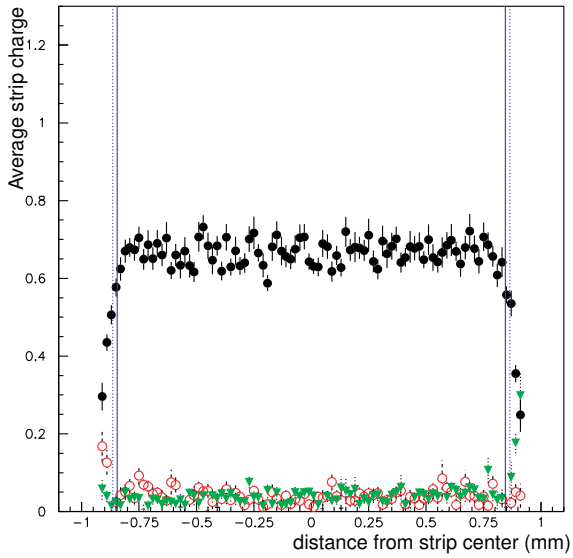

Figure 37: Average strip charge as a function of the distance to the centre of the central strip for Elma D2-1-n+ at 150V.

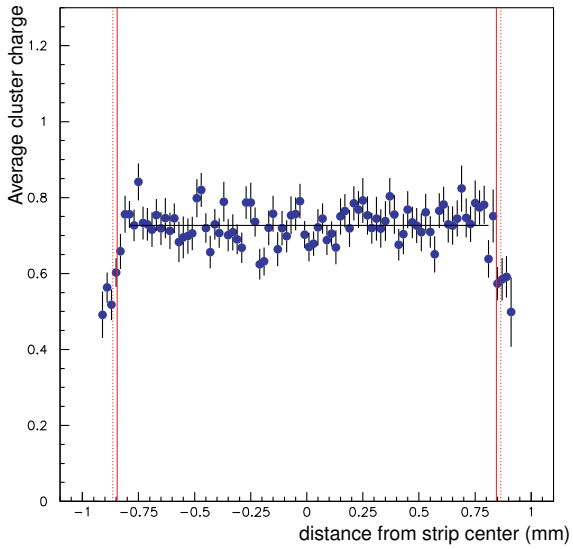

Figure 38: Average cluster charge as a function of the distance to the centre of the central strip for Elma D2-1-n+ at 150V.

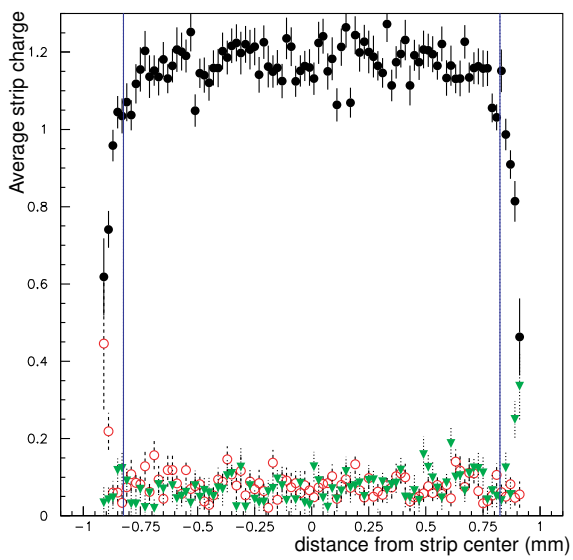

Figure 39: Average strip charge as a function of the distance to the centre of the central strip for Demokritos N5 at 600V.

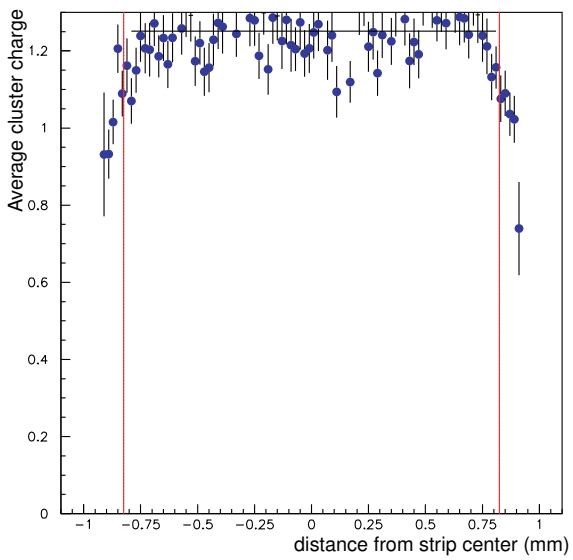

Figure 40: Average cluster charge as a function of the distance to the centre of the central strip for Demokritos N5 at 600V.

probable value or their average, the latter being more convenient in the case of small statistics. The most probable value is obtained through a local Gaussian fit of the maximum of the distribution.

When trying to compare the two regions, there is a difficulty in the definition of the cluster. We have used two possibilities:

- a 3 strips cluster centred around the central strip for the case where the particle hits inside the implant and a 2 strips cluster (one on each side) for an impact in the inter-strip region. This choice is very logical but may introduce a systematic difference between the two cases.
- a 4 strips cluster for both cases, which is a more symmetric definition. In the case of the central impact, the fourth strip is the nearest to the particle impact.

Figs 41 to 43 show the results as a function of the p^+-p^+ distance for several detectors.

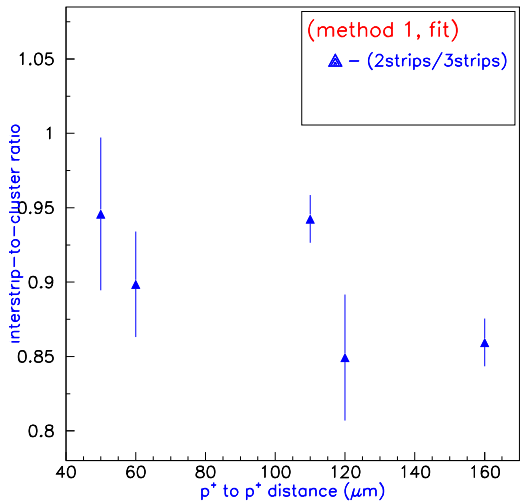

Figure 41: Ratio of most probable charge value between inter-strip and central region as a function of the p^+-p^+ distance (clusters of 2 and 3 strips respectively).

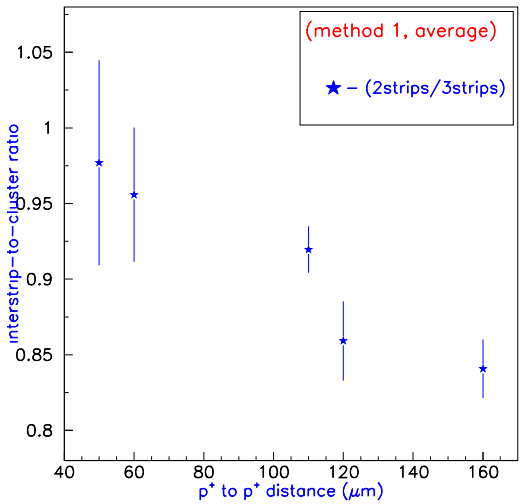

Figure 42: Ratio of average charge value between inter-strip and central region as a function of the p^+-p^+ distance (clusters of 2 and 3 strips respectively).

There is an effect in all cases. For a p^+ - p^+ distance of $50\mu m$ the charge is practically independent of the position. For large gaps, as much as 15% charge can be lost in the region between the implants. Electron showers have a very narrow spatial distribution: for example, an average of 32% of the energy is deposited in a $95\mu m$ wide region for a 120 GeV electron after 2 X^0 [1]. Therefore a charge loss in the inter-strip region can introduce a non-negligible spatial non-uniformity in the detector response if the inter-strip region is too large. This effect has to be considered in the sensor specifications.

8.2 Cross talk

As can be seen from on Figures 19 to 33, the charge on the left and right neighbour strips is not vanishing but has an average level of the order of 5%, irrespective of the particle position. This effect is not due to an electronics cross talk (we checked it without detector), but to the inter-strip capacitance. This explanation is sustained by Figure 44, which shows that the fractional charge observed in the neighbour strip decreases with increasing inter-strip distance. For the next two neighbours, the induced charge is very small (typically $\leq 0.5\%$).

8.3 Charge collection near the guard ring

Figure 45 and 46 show the average charge as function of position for the guard ring region of two detectors, Demokritos-N5 and Taiwan45-5, running both along (x) or across (y) the strips. The shape is the same in both directions. The charge collection extends to the guard ring region, being still 50% 300 μm away from strip edge.

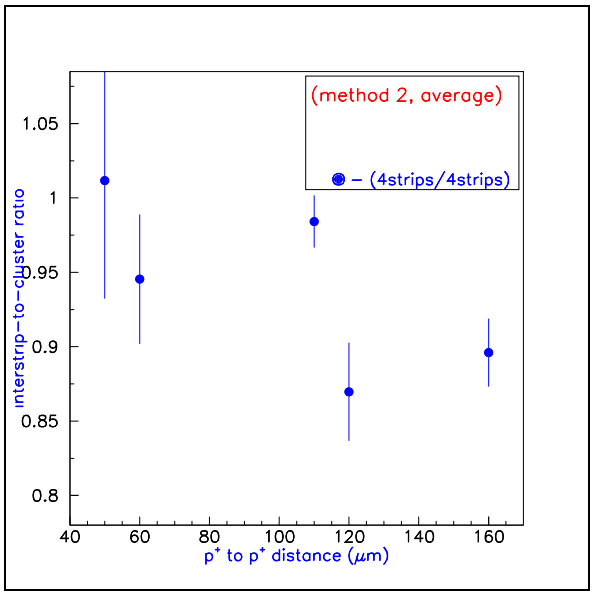

Figure 43: Ratio of average charge value between interstrip and central region as a function of the p^+-p^+ distance (clusters of 4strips).

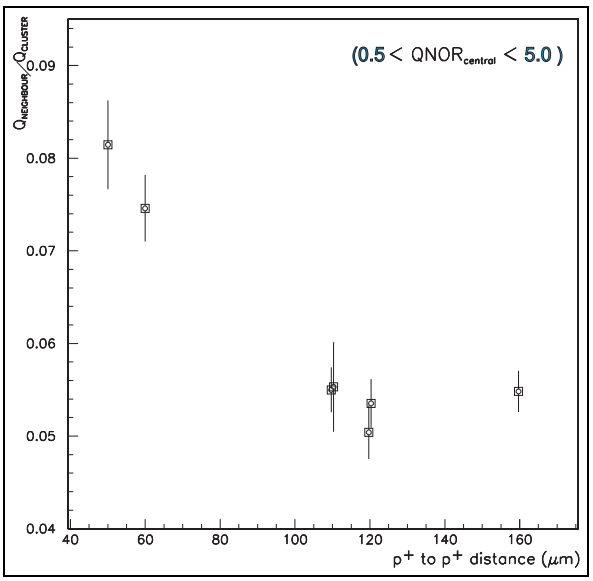

Figure 44: Fraction of charge in the neighbour strip vs. inter-strip distance

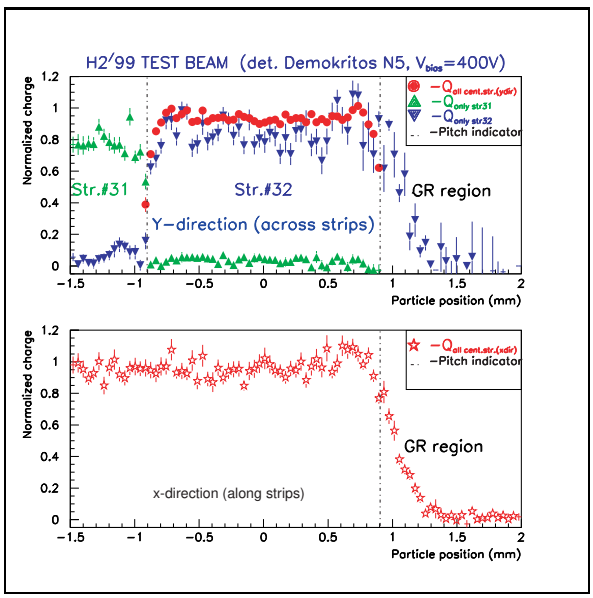

Figure 45: CCE versus particle hit position for y-direction and x-direction for Demokritos N5

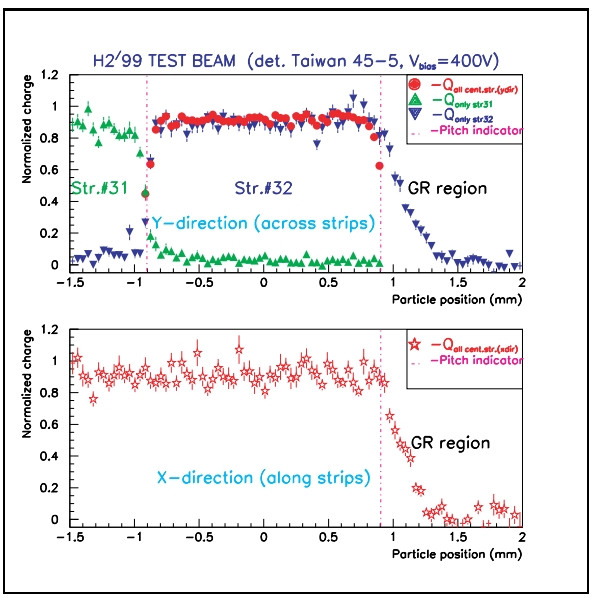

Figure 46: CCE versus particle hit position for y-direction and x-direction for Taiwan 45-5.

This effect increases slightly the active area of the detector. Figure 47 and 48 show the charge distribution in the guard ring region as function of bias voltage. On the efficiency plateau the effect is independent of bias.

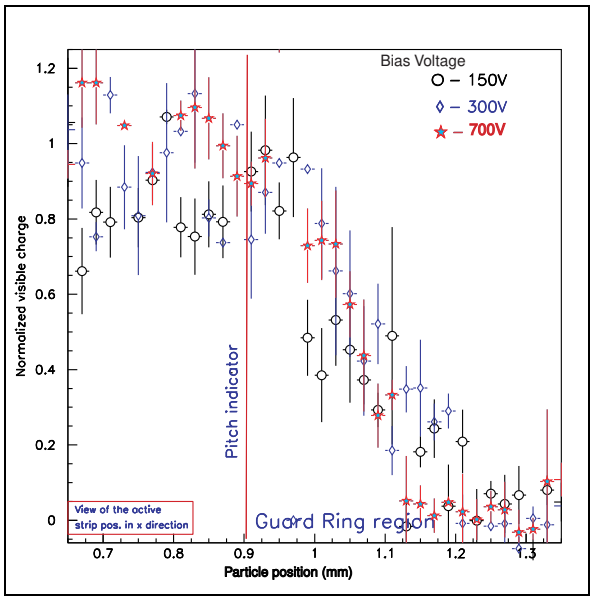

Figure 47: CCE versus a particle position in x-direction by different bias voltage for Hamamatsu 15

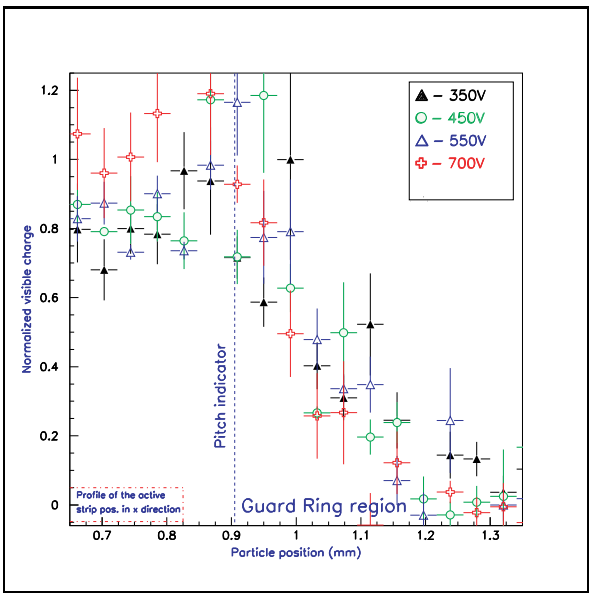

Figure 48: CCE versus a particle position in x-direction by different bias voltage for Taiwan 45-5.

9 Signal to noise ratio

We have measured the signal to noise ratio for the various detectors on efficiency plateau. It is defined as the ratio of the central strip charge to the strip noise. The measurements are reported in Table 2. Due to the non uniformity of the electronics , there are fluctuations from channel to channel (see Figures 49 or 50) and a systematic error of ± 0.5 should be quoted for these values. The irradiated detectors have a signal to noise ratio close to 6, except for the thicker ones which have, as expected, a better performance.

Table 2: Signal to noise ratio

Detector	bias voltage (V)	S/N	Fluence $\times 10^{14} cm^{-2}$	Thickness (μm)
Hamamatsu 8	500	6.5	0	313
Taiwan 45-5	400	6.0	3.1 p	338
Hamamatsu 15	700	6.5	1.2 n	311
Elma N9-1	450	5.6	3.2 p	300
Elma d2-1-n+	300	6.	1.2 n	308
Elma DSP7	600	7.5	2.3 n	382

We recall that the SCT32 chip is not optimised for our large capacitance detectors. The expected SCT noise is $\sim$ 3400 e$^-$ for the $60 \times 60 mm^2$ detectors whose total capacitance/strip is around $44pF$ and $\sim$ 3800 e$^-$ for the $63 \times 63 mm^2$ detectors whose capacitance is $50pF$ [6]. The mip signal for a $300\mu m$ thick detector is 25000 e$^-$. Taking into account the loss of the charge in the neighbour strips, we expect a signal to noise of 6.6 (resp 5.9) for small (resp. large) sensors at 100% charge collection efficiency. Our results are in agreement with these expectations.

Figure 49 and 50 show the evolution of the signal to noise ratio for Ham8 (non-irradiated) and Ham15 (irradiated) with bias voltage. There is no indication of a deterioration at very high bias values. Figure 51 shows the signal to noise ratio for the two geometry options of the Taiwan detector. At 400 V bias, the average signal to noise ratio is 6.05 in the 50μm inter-strip distance region and 6.35 in the 160μm inter-strip distance region.

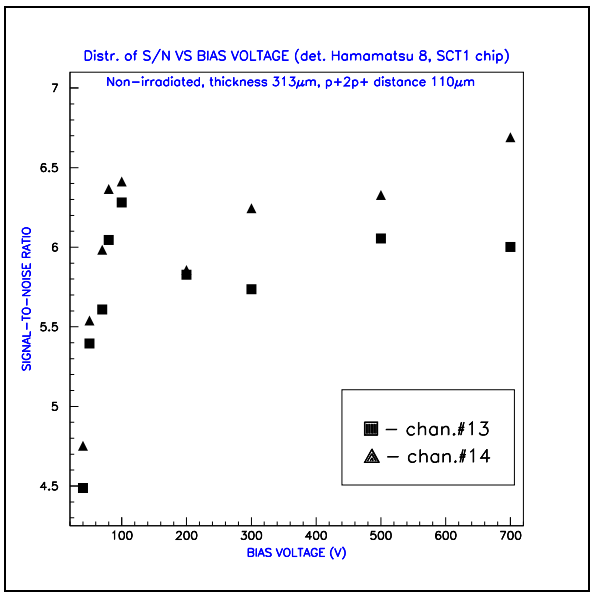

Figure 49: Distribution of the signal-to-noise ratio versus bias voltage of the selected readout strip for Hamamatsu 8.

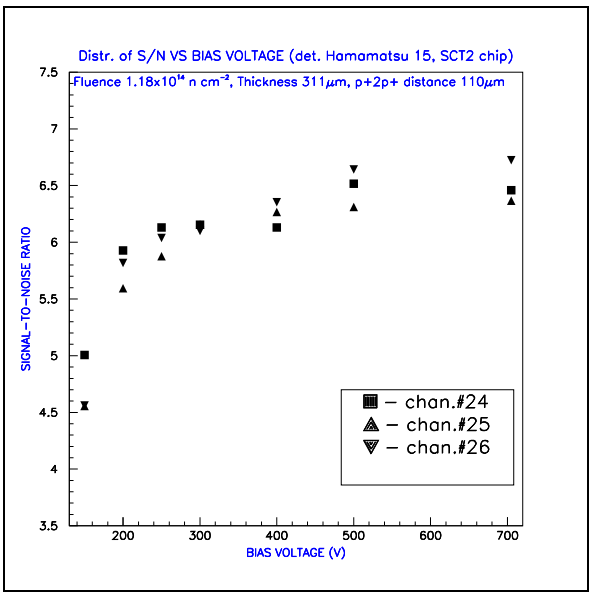

Figure 50: Distribution of the signal-to-noise ratio versus bias voltage of the selected readout strip for Hamamatsu 15.

However, due the the large channel to channel non uniformity, it is hard to draw a firm conclusion.

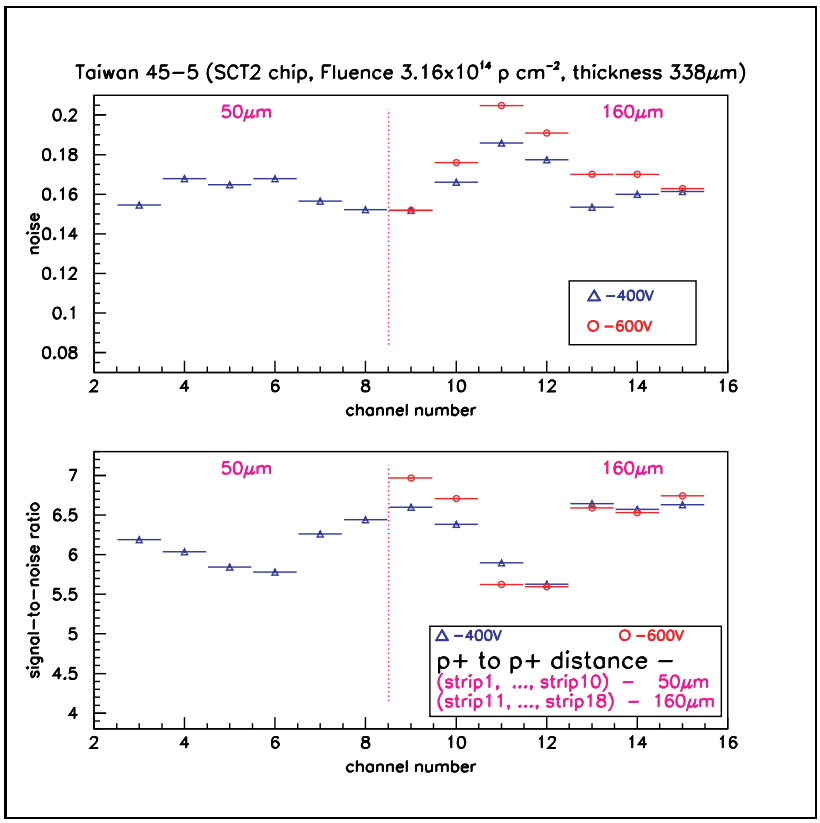

Figure 51: Noise and signal-to-noise ratio as a function of the strip number. The dotted line shows the boundary between the regions with different p^+ to p^+ distance)

10 Conclusions

Thanks to the high precision telescope, details of the charge collection efficiency have been studied for irradiated detectors. The results agree with previous results obtained in the laboratory with a radioactive source setup. In all the cases, we find working conditions with high charge collection efficiency. The charge collection in the inter-strip region increases for decreasing inter-strip distances, yielding better spatial uniformity for small distances . However in this case the inter-strip capacitance (and therefore both the noise [6] and the cross talk with neighbour strips) increases for smaller distances. These two effects have to be compromised in the final specification.

11 Acknowledgements

We are thankful to P.V. Moissenz for his useful constructive discussion and remarks to the data process.

References

[1] A. Peisert et al.,"Silicon detectors for the CMS Preshower", CMS NOTE-2000/061

[2] Ph. Bloch et al., "Performance study of non-irradiated prototype silicon preshower samplers for CMS", CMS TN/2000-042.

[3] O. Toker et al., Nucl. Instr. and Meth. A 340 (1994) 572; manufacturer: IDE AS, Gaustadalleen 21, N-0371 Oslo, Norway.

[4] F. Anghinolfi et al., "SCTA - A rad-hard BiCMOS anolog readout ASIC for ATLAS semiconductor tracker", IEEE Trans. Nucl. Sci., vol. 44, No. 3, 298-302 (1997).

[5] A. Cheplakov et al., "Radiation hardness of GaAs preamplifiers for liquid argon calorimetry at LHC", MPI Report, PhE/96-15.

[6] A. Go and A. Peisert, "Measurement of the capacitance of Preshower detectors", CMS IN-2000/041